Resolving the Rise and Fall of Star Formation in Galaxies
Proceedings IAU Symposium No. 373, 2023
T. Wong & W.-T. Kim, eds.
doi:10.1017/S1743921323000157

Star Formation History in the Illustris TNG Simulation

András Péter Joó[1], Bendegúz Koncz[1], Sandor Pinter[2] and L. Viktor Tóth[1]

[1]Dept. of Astronomy, Eötvös Loránd University

[2]Dept. of Natural Science, University of Public Service, Hungary

Abstract. We processed the catalogue data for all snapshots of the Illustris TNG100 cosmological simulation and collected every calculated property of the galaxies formed at different redshifts. With this dataset we can statistically analyze parameters for galaxy samples at given redshifts, as well as trace sample parameters over the entire time range of the simulation. Focusing first on star formation rate (SFR) and metallicity, we see the cosmic star formation history with the mean maximum at around $z \approx 1.6$ and the reionization bump at around $z \approx 5$, while metallicity increases. For a sample of strongly star-forming galaxies with SFR > 10 $M_{\odot}yr^{-1}$ we found different characteristics compared to the whole sample. The mean metallicity of highly star-forming galaxies is higher and changes less, and the mean SFR has its maximum at around the reionization bump.

Keywords. software: simulations, galaxies: star formation, galaxies: starburst, galaxies: high-redshift

1. Introduction

IllustrisTNG (Springel et al. (2018), Marinacci et al. (2018), Nelson et al. (2018), Pillepich et al. (2018), Naiman et al. (2018)) is a suite of large volume, cosmological, gravo-magneto-hydrodynamical simulations including a comprehensive model for galaxy formation. Each TNG simulation self-consistently solves for the coupled evolution of dark matter, cosmic gas, luminous stars, and supermassive blackholes from redshift $z = 127$ to 0 and generates 100 resulting snapshots from $z = 20$ to 0. We used the TNG100 run for analysis, the main high-resolution run including the full TNG physics model, which has the size of 110.73 Mpc^3 and contains more than 10 billion resolution elements.

2. Data processing and results

We processed the catalogue data for all snapshots of the TNG100 run to statistically analyze the properties of galaxies at each redshift. We collected every property from the catalogue files for all the subhalos found by the subfind algorithm, so that we have the subhalo-level properties for all the galaxies exported for every snapshot. With this dataset it becomes possible not only to statistically analyze parameters for galaxy samples at given redshifts, but to easily trace sample parameters over the entire time range of the simulation.

Here we are focusing on how the star formation rate (SFR) and metallicity ($\not{Z}$) of galaxies evolved through time (redshift z). The SFR is calculated for every subhalo from the star formation processes. The metallicity is calculated as $\not{Z} = M_Z/M_{tot}$ of all gas cells bound to the subhalo, where Z is any element above He. The star formation rate

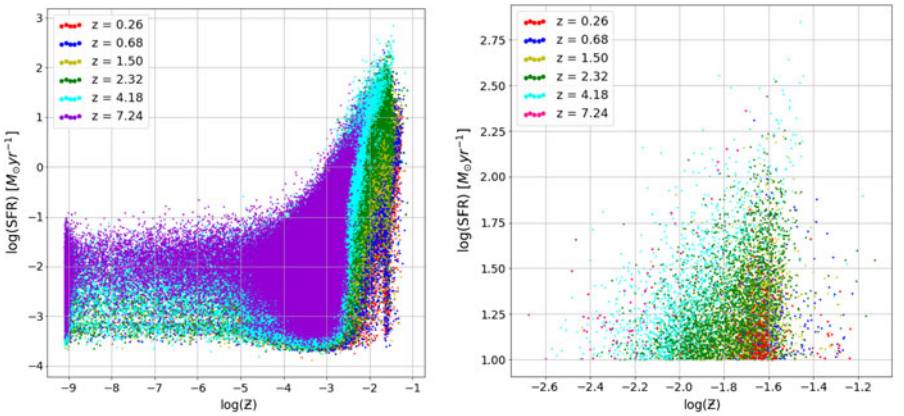

Figure 1. The relation between star formation rate (SFR) and metallicity (Ƶ) for individual galaxies at different redshifts in the TNG100 simulation. Left: all galaxies in the snapshots. The whole population spreads towards lower SFR at low metallicities and higher SFR at higher metallicities, while new higher metallicities appear. Right: galaxies with SFR > 10 $M_\odot yr^{-1}$. Strongly star-forming galaxies are located at high metallicities, and tend towards lower SFR and higher metallicity.

density (SFRD) is calculated as the sum of SFRs for all galaxies in a sample divided by the simulation volume 1000Mpc^3. The mean star formation rate (<SFR>) is the average of the SFRs for all galaxies in a sample.

Besides investigating the whole galaxy sample in each redshift, we also separated galaxies with SFR > 10 $M_\odot yr^{-1}$ as a crude sample for strongly star-forming galaxies.

Figure 1 shows parameters of individual galaxies in six snapshots from z = 7.24 to z = 0.26. The diagram on the left includes all galaxies, while the one on the right contains only strongly star-forming galaxies with SFR > 10 $M_\odot yr^{-1}$. The whole population spreads towards lower SFR at low metallicities and higher SFR at higher metallicities, while new higher metallicities appear. Strongly star-forming galaxies are located at high metallicities for all the six redshifts, and tend toward lower SFR and higher metallicity.

Figure 2 shows the change of star formation rate density (SFRD) and mean metallicity through cosmic time, the left diagram shows data for all galaxies, while the right diagram shows data only for strongly star-forming galaxies with SFR > 10 $M_\odot yr^{-1}$. The cosmic trend of star formation rate density can be seen, in accordance with previous results from the Illustris simulation (eg. Bignone et al. (2017)). We have our highest data point at z = 2.73. Strongly star-forming galaxies show similar trend with a noticeable bump from z $\approx$ 6 to 4, a period after the reionization epoch (Bauer et al. (2015), Thélie et al. (2022)).

We can observe this bump in detail looking at the mean SFR on Figure 3, on the left for all galaxies, and on the right for galaxies with SFR > 10 $M_\odot yr^{-1}$. Strongly star-forming galaxies have their peak <SFR> after the reionization epoch, from z $\approx$ 6 to 4, and a relapse can also be seen around z $\approx$ 7.

3. Summary and discussion

We investigated how the star forming rate (SFR) and metallicity of galaxies evolve through time (redshift z) in the Illustris TNG100 simulation. We found that the galaxy population spreads towards lower SFR at low metallicities and high SFR at high metallicities, while strongly star-forming galaxies with SFR > 10 $M_\odot yr^{-1}$ tend towards lower SFR and higher metallicity. The star formation density shows the cosmic trend in accordance with previous results from the Illustris simulation (eg. Bignone et al. (2017)) with

https://doi.org/10.1017/S1743921323000157 Published online by Cambridge University Press

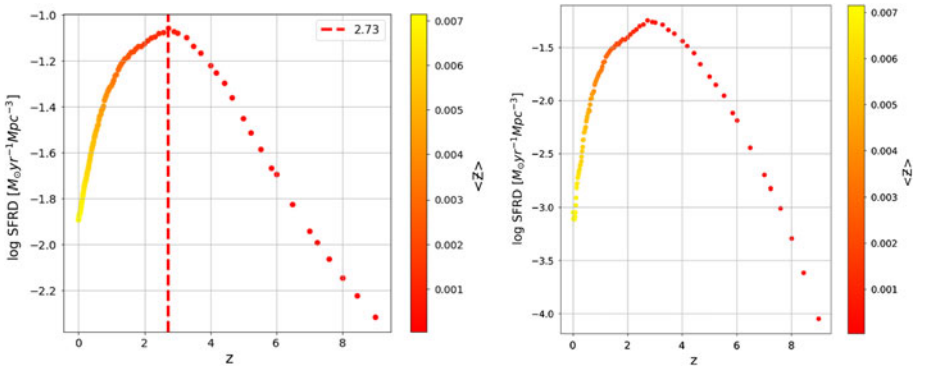

Figure 2. The change of the star formation rate density (SFRD) and mean metallicity (Ƶ) with redshift (z) in the TNG100 simulation. Left: for all galaxies in the snapshots. The cosmic trend of SFRD can be seen with the highest data point at z = 2.73. Right: for strongly star-forming galaxies with SFR > 10 $M_\odot yr^{-1}$. Similar trend with a bump after the reionization epoch between z ≈ 6 to 4.

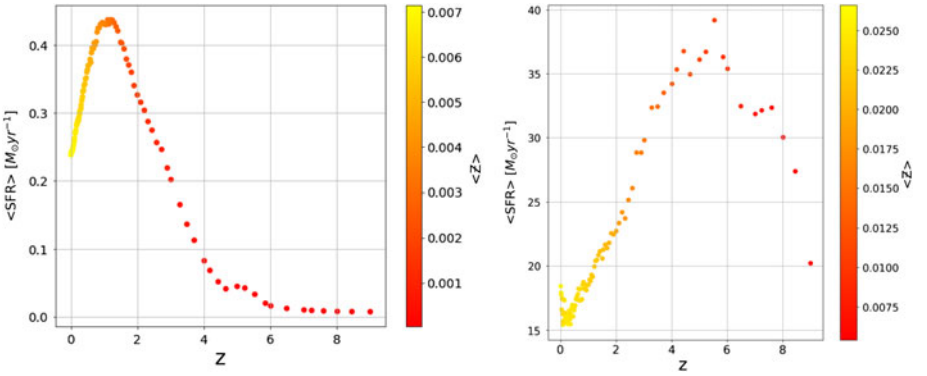

Figure 3. The change of the mean star formation rate (<SFR>) and mean metallicity (Ƶ) with redshift (z) in the TNG100 simulation. Left: for all galaxies in the snapshots. A bump can be seen after the reionization epoch from z ≈ 6 to 4. Right: for strongly star-forming galaxies with SFR > 10 $M_\odot yr^{-1}$. <SFR> peaks after the reionization epoch from z ≈ 6 to 4.

a noticeable bump after the reionization epoch (Bauer et al. (2015), Thélie et al. (2022)) from z ≈ 6 to 4 for strongly star-forming galaxies, that can be further observed looking at how the mean SFR changes with redshift. Strongly star-forming galaxies have their peak mean SFR in the z ≈ 6 to 4 period, and also a relapse can be seen around z ≈ 7.

Current models suggest that strongly star-forming environments produce more Long Gamma Ray Bursts (LGRBs). With the use of our dataset we plan to validate these models by assembling possible LGRB host galaxy samples and compare those with results from observational data (for eg. Rácz et al. (2018), Tóth et al. (2019), Horvath et al. (2022)).

Acknowledgements

Simulation data is provided by The TNG Collaboration: https://www.tng-project.org/. This work was supported by the Hungarian TKP2021-NVA-16 grant.

https://doi.org/10.1017/S1743921323000157 Published online by Cambridge University Press

Supplementary material

To view supplementary material for this article, please visit https://doi.org/10.1017/S1743921323000157.

References

Springel et al. 2018. MNRAS, 475, 676. doi:10.1093/mnras/stx3304
Marinacci et al. 2018. MNRAS, 480, 5113. doi:10.1093/mnras/sty2206
Nelson et al. 2018. MNRAS, 475, 624. doi: 10.1093/mnras/stx3040
Pillepich et al. 2018. MNRAS, 475, 648. doi: 10.1093/mnras/stx3112
Naiman et al. 2018. MNRAS, 477, 1206. doi: 10.1093/mnras/sty618
Bignone et al. 2017. MNRAS, 469, 4921. doi: 10.1093/mnras/stx1132
Bauer et al. 2015. MNRAS, 453, 3593. doi: 10.1093/mnras/stv1893
Thélie et al. 2022. A&A, 658, A139 doi: 10.1051/0004-6361/202141748
Rácz et al. 2018. AN, 339:347–351. doi.: 10.1002/asna.201813503
Tóth et al. 2019. MNRAS, 486, 4823. doi.: 10.1093/mnras/stz1188
Horvath et al. 2022. Universe, 8(4), 221. doi: 10.3390/universe8040221